Mode Selective Control of Drift Wave Turbulence

Christiane Schröder and Thomas Klinger
Institut für Physik, Ernst-Moritz-Arndt Universität, Greifswald, Germany

Dietmar Block and Alexander Piel
Institut für Experimentelle und Angewandte Physik, Christian-Albrechts Universität, Kiel, Germany

Gérard Bonhomme
Laboratoire de Physique des Millieux Ionisés, Université Henri Poincaré, Nancy, France

Volker Naulin
Risø National Laboratory, Roskilde, Denmark
(Received 12 October 2000)

Experiments on spatiotemporal open-loop synchronization of drift wave turbulence in a magnetized cylindrical plasma are reported. The synchronization effect is modeled by a rotating current profile with prescribed mode structure. Numerical simulations of an extended Hasegawa-Wakatani model show good agreement with experimental results.

DOI: 10.1103/PhysRevLett.86.5711 PACS numbers: 52.35.Kt, 05.45.Xt, 52.35.Ra

Drift waves are caused by pressure-driven instabilities in magnetized plasmas [1]. Drift wave turbulence is generally believed to be responsible for anomalous cross-field particle transport [2] and it is an appealing long-term perspective to influence systematically the turbulent transport in magnetically confined plasmas by *active* control of drift wave dynamics. As drift wave turbulence is basically a spatiotemporal phenomenon, it is barely expected that a purely temporal or spatial control technique proves to be efficient and robust. A number of experiments on temporal feedback control of plasma instabilities were reported [3] but often with ambiguous conclusions. In general, the goal of control can be either suppression or stabilization of given dynamics. The suppression of several drift-type instabilities was recently demonstrated in a linear magnetized device [4]. Control of chaos [5] is a different approach, where unstable periodic states are stabilized by tiny adjustments of one or more accessible parameters. The success of this conception was demonstrated for various different plasma waves and instabilities [6]. Drift wave chaos was successfully controlled by temporal feedback [7], but in drift wave dynamics low-dimensional chaos exists only in a narrow regime of the transition route to turbulence [8].

We follow a recently proposed stabilization strategy: open-loop control (synchronization) acting in both space and in time [9]. It turns out that drift wave turbulence is reduced by driving preselected drift modes to the expense of the broadband spectrum. Experiments and numerical simulations were conducted for a magnetized plasma with cylindrical geometry. For the synchronization experiments, an arrangement of eight stainless-steel electrodes (octupole exciter) is positioned in flush-mounted geometry in the edge region of the plasma column (Fig. 1). The electrodes of the octupole exciter are driven by sinusoidal signals with a fixed, preselected phase angle θ between each electrode pair. In this way, an azimuthally rotating electric field is generated. The numerical simulations are based on an extended Hasegawa-Wakatani model in 2D disk geometry, with the ultimate goal to identify the basic physical mechanism how the external synchronization signal is coupled to the drift wave dynamics. Both experiment and numerical simulation show that relatively weak exciter signals synchronize turbulent drift wave states and thereby establish a preselected single drift mode.

The experiments are carried out in the linear, magnetized, low-β plasma device MIRABELLE [10]. It consists of two plasma source chambers and a magnetized midsection (length 1.4 m, column diameter 0.30 m, magnetic field $B = 40-100$ mT). Argon plasma is produced in the source chambers by thermionic hot-cathode discharge in steady-state operation (neutral gas pressure $p = 3 \times 10^{-4}$ mbar, electron temperature $T_e = 1.2-3.5$ eV, electron density $n_e = 2 \times 10^{16}$ m^{-3}). Each source chamber

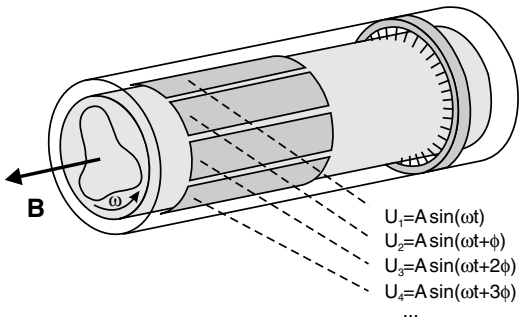

FIG. 1. The octupole exciter is a circular arrangement of eight stainless-steel plates of length 32 cm with a 2 mm gap between each two neighboring plates. The radius of the exciter is $r_x = 10$ cm. Spatiotemporal drift wave dynamics is measured with an azimuthal Langmuir probe array.

is separated from the midsection by a stainless-steel mesh grid (transparency >60%). Only one chamber is operated as a plasma source. The grid at the active chamber is positively biased while the other grid, acting as loss surface, is kept at ground potential. In this way electrons are injected into the midsection and, to a certain degree, an $\mathbf{E} \times \mathbf{B}$ rotation of the plasma column is established [11]. The magnetized plasma column is immersed in a stainless-steel tube, which is positively biased to predefine the potential at the azimuthal boundary (potential range $U_t = 0{-}20$ V). Further information about the experiment is found in Refs. [7] and [11].

Drift waves propagate azimuthally in the magnetized plasma column due to fluctuation-induced $\mathbf{E} \times \mathbf{B}$ drift in the presence of a radial density gradient. Control parameters for drift wave dynamics are the grid bias U_g and the tube bias U_t. Both biases superimpose a radial electric field across the plasma column and thereby an $\mathbf{E} \times \mathbf{B}$ rotation, which is known to destabilize drift waves [12]. Increasing either U_g or U_t leads to a transition scenario from a stable plasma state to drift wave turbulence [8]. The spatiotemporal drift wave dynamics is observed using a circular array of 32 equally spaced cylindrical Langmuir probes [13], operated in the electron saturation current regime to measure density fluctuations (Fig. 1).

The first step in experiment is to establish stationary, fully developed drift wave turbulence. This is achieved by choosing values $U_g = 5$ V and $U_t = 12$ V and the result is depicted in Figs. 2(a)–2(d). The time trace of the floating potential fluctuations (a) is clearly irregular and the corresponding frequency power spectrum $S(f)$ is broadband (b), even though a few pronounced peaks are visible in the low-frequency regime ($f < f_{ci} = 15$ kHz, the ion cyclotron frequency). We note that such low-frequency peaks have previously been observed for drift wave turbulence in plasmas with cylindrical geometry [14]. The spatiotemporal data (c), obtained with the probe array, are dominated by irregular features and no clear-cut mode structure is observed [8,11]. Developed turbulence is further corroborated by the frequency-mode-number spectrum $S(f, m)$, shown in Fig. 2(d). Spectral components are scattered over a broad area in the (f, m) plane and show no unique dispersion relation.

For synchronization of drift wave turbulence, a driver frequency f_d is chosen to be close to pronounced spectral features in the low-frequency regime. An azimuthal mode number m_d is predetermined by selecting a phase shift $\theta = m_d \pi/4$. Nyquist's sampling theorem restricts the mode number range to $m_d = 1, 2, 3$. The so-obtained exciter signal drives a specific drift mode with phase velocity $v_\phi = f_d \times 2\pi r_x/m_d$, which must be compatible with the drift wave dispersion. r_x is the radial position of the exciter electrodes. Choosing $m_d = 2$, driver frequency $f_d = 8.0$ kHz, and driver amplitude $A = 1.0$ V the above discussed drift wave turbulence is successfully synchronized as shown in Figs. 2(e)–2(h). The floating potential fluctuations (e) are now fairly regular and have a relatively large amplitude, of the order of the largest events in the turbulent state [cf. Fig. 2(a)]. The frequency power spectrum (f) is sharply peaked at 8.06 kHz and its higher harmonics only, meaning that the preselected mode is enhanced to the expense of broadband low-frequency spectral components. The spectral index $f^{-\alpha}$ of the broadband high-frequency underground ($f \geq f_{ci} = 15$ kHz, small-scale) drops from $\alpha = 4.2$ to $\alpha = 3.5$. Synchronization increases the integrated fluctuation power by a factor of

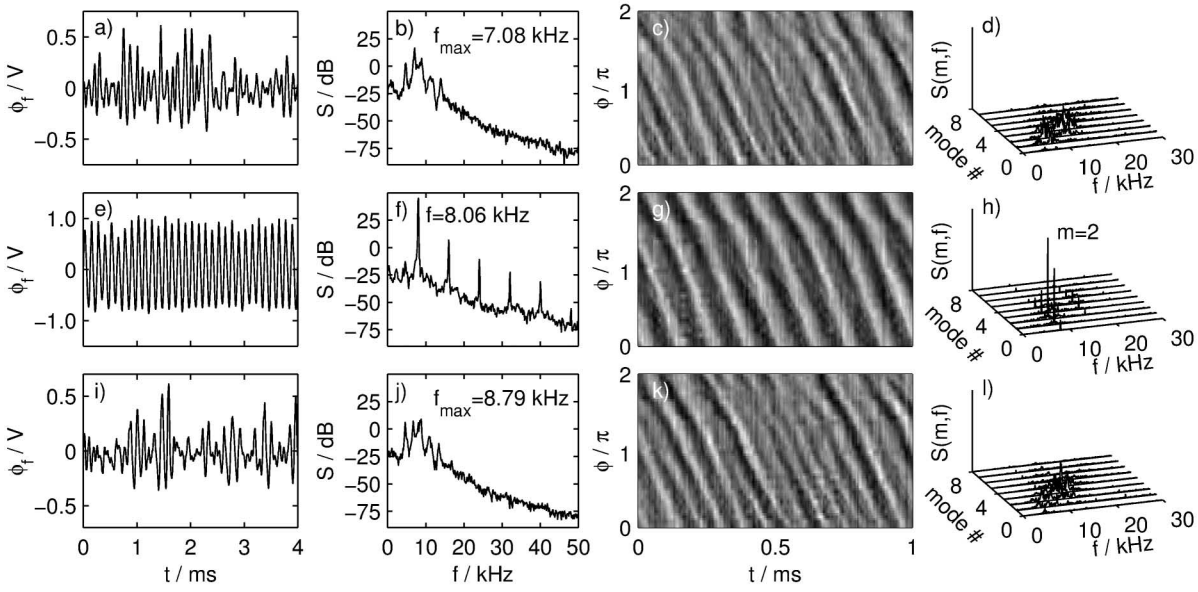

FIG. 2. Temporal and spatiotemporal drift wave dynamics: experiment. The three rows correspond to the unperturbed case, active exciter with a corotating field, and active exciter with a counterrotating field, respectively. The four columns show the floating potential fluctuations, the frequency power spectrum, the spatiotemporal density fluctuations, and the frequency-mode-number power spectrum. Power spectra are obtained by Fourier transform of the temporal and spatiotemporal data.

5.7, where increase is due to the driven mode whereas the power of the broadband part is significantly decreased. Regular dynamics dominate the spatiotemporal data (g) as well. A pronounced wave structure with mode number $m = 2$ is found, which is also present in the sharply peaked frequency-mode-number spectrum $S(f, m)$. This further emphasizes the mode-selective character of the spatiotemporal control of the drift wave turbulence.

To test if the control effect is really spatiotemporal, we reverse the sign of θ and thus the rotation direction of the exciter field. In contrast to the corotating case described above, the counterrotating exciter signal is moving at $\sim 2v_\phi$ in the drift wave frame. If the synchronization is an actual spatiotemporal effect, we expect a much weaker influence for counterrotating excitation than for a corotating one. Figures 2(i)–2(l) show the result. Indeed, the counterrotating exciter field has almost no influence on the drift wave turbulence. Note that, except for the sign of θ, all parameters are kept the same. The floating potential fluctuations (i), frequency power spectrum (j), spatiotemporal data (k), and the frequency-mode-number spectrum are barely distinguished from the unperturbed case (a)–(d). In conclusion, the interaction between the counterrotating exciter field and the drift wave turbulence is weak, as expected. This emphasizes the importance of spatiotemporal synchronization in the present experiments.

We have performed similar synchronization experiments for several different drift wave turbulence regimes, always with the same result. Probe measurements in the exciter region have shown that the actual perturbation of the plasma equilibrium by the exciter field is in the range of a few percent. Turbulence synchronization is also possible for different preselected mode numbers in the range $m_d = 1$–3 (with appropriately chosen f_d), but $m_d = 2$ requires the lowest driver amplitude. Driving a single electrode with signals of the same amplitudes gave almost no effect.

For the numerical simulations we consider a standard drift wave model, the Hasegawa-Wakatani equations [15] for density and vorticity fluctuations, which we write in the form with retained parallel current as

$$\frac{\partial}{\partial t}\nabla_\perp^2\phi + \vec{V}_{\mathbf{E}\times\mathbf{B}}\cdot\nabla\nabla_\perp^2\phi = \nabla_\parallel J_\parallel + \mu_w\nabla_\perp^4\phi\,, \quad (1)$$

$$\frac{\partial}{\partial t}n + \vec{V}_{\mathbf{E}\times\mathbf{B}}\cdot\nabla(N_0 + n) = \nabla_\parallel J_\parallel + \mu_n\nabla_\perp^2 n\,, \quad (2)$$

with $J_\parallel = -\sigma\nabla_\parallel(\phi - n)$. Here we employed the usual drift scale ordering and have made the equations dimensionless using ρ_s and Ω_i as typical length and frequency scales [16]. σ is the suitably normalized parallel conductivity and N_0 is the fixed background density profile. Note that we do not employ the local approximation for the density gradient.

The exciter itself is modeled by assuming that it gives rise to an additional oscillatory parallel current profile of the functional form $\nabla_\parallel J_{\text{ext}} = A\sin(\pi r/r_0)\sin(2\pi m_d\Theta - \omega_d t) = S$, where r_0 is the radius of the plasma and Θ is the poloidal coordinate. Making the transition to a 2D model we arrive at

$$\frac{\partial}{\partial t}\nabla_\perp^2\phi + \vec{V}_{\mathbf{E}\times\mathbf{B}}\cdot\nabla\nabla_\perp^2\phi = \tilde{\sigma}(\phi - n) - S + \mu_w\nabla_\perp^4\phi\,, \quad (3)$$

$$\frac{\partial}{\partial t}n + \vec{V}_{\mathbf{E}\times\mathbf{B}}\cdot\nabla(N_0 + n) = \tilde{\sigma}(\phi - n) - S + \mu_n\nabla_\perp^2 n\,, \quad (4)$$

where we used $\nabla_\parallel^2 \approx -k_\parallel^2$, and $\tilde{\sigma} = k_\parallel^2\sigma = k_\parallel^2\rho_s T_e/m_e c_s \nu_{ei}$. Additionally, in small layers around $r = 0$ and

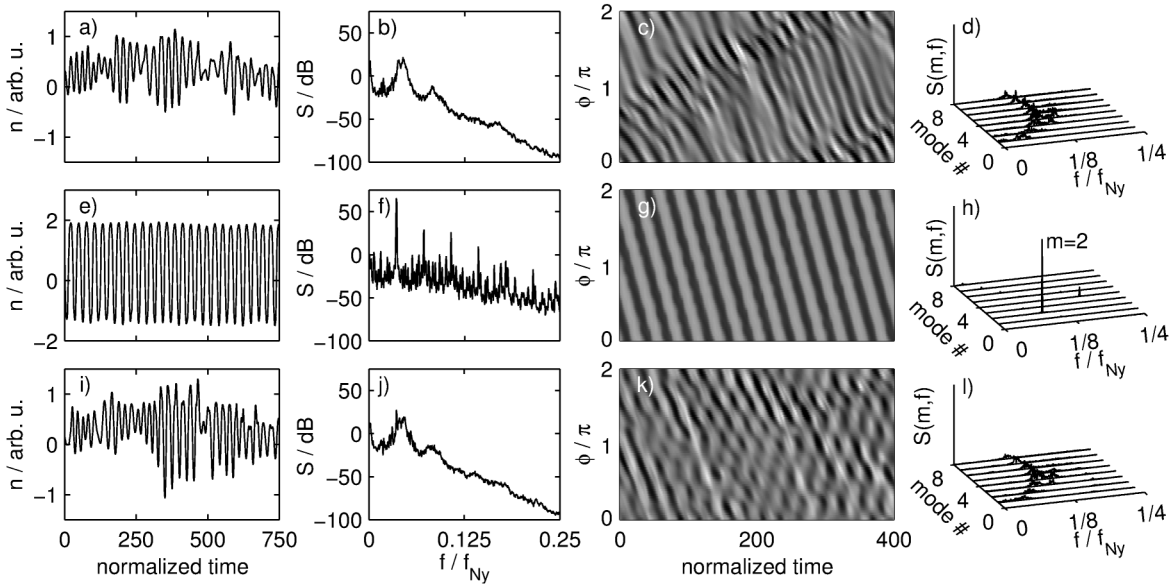

FIG. 3. Temporal and spatiotemporal drift wave dynamics: simulation. The figure is arranged as in Fig. 2 and the same diagnostic tools are used. Good agreement is found between experiment and simulation. $f_{Ny} = 1/2\Delta t$ is the Nyquist frequency. The ion cyclotron frequency is found to be in the frequency range carrying the main spectral power.

$r = r_0$ the viscosities were enhanced by a factor of 200. These layers act as sources and sinks and sustain the background density gradient. Equations (3) and (4) are solved using the Arakawa scheme [17] to discretize nonlinearities and density background term and second-order centered finite differences for the remaining terms. For time stepping a third-order stiffly stable splitting method is used [18]. Simulations are performed in poloidal coordinates on a disk, with typically up to 64×128 grid points in the radial and the poloidal direction, respectively. The density profile is taken to be of the form $N_0 = 2.5\cos(r/r_0)$, with $r_0 = 10$ and the viscosities $\mu_{n,w}$ are of order 10^{-3} and $\tilde{\sigma} = 0.1$. The parameters are chosen to establish a saturated turbulent state similar to the experimentally observed one. Time series of the density and potential fluctuations are analyzed using the same diagnostic tools as for the experimental data.

The simulation result is shown in Fig. 3. By comparing Figs. 2 and 3 it becomes evident that the experimental findings discussed above are fully reproduced by the simulation. Starting with unperturbed drift wave turbulence (a)–(d), a synchronized $m = 2$ state is achieved at a relatively small driver amplitude, $A = 0.75$, if a corotating current profile is applied (e)–(h). Exactly as in the experiment, a counterrotating current profile of the same amplitude has almost no effect (i)–(l). The integrated spectral power and spectral indices behave similar to experiment. For synchronized turbulence, the integrated spectral power is increased by a factor of 5.5 and the spectral index α drops by a factor of 2–3, stronger than in experiment. From numerical simulation we may conclude that the experiment is at least qualitatively reproduced by the 2D model (3) and (4). The rotating current profile couples via $\nabla_{\parallel} J_{\text{ext}}$ the two equations mode selectively and thus leads to amplification of the preselected mode m_d. In other words, in the drift wave frame the poloidal symmetry is broken by the structured current profile which leads to mode selection. We note that only a rotating current profile yields synchronization; alternative concepts like rotating electric fields, etc., gave no effect.

Full access to the poloidal plane allows one to inspect the drift mode structure for the three cases (Fig. 4). In the synchronized case a clear $m = 2$ mode structure is recognized, whereas in the other two cases smaller scale irregular structures prevail. Note that simulations may give insight into further interesting points, e.g., systematic change of anomalous particle transport. This should be done, however, in 3D and results will be reported in a later publication.

In conclusion, mode-selective control of drift wave turbulence by spatiotemporal synchronization was demonstrated. In experiment synchronization was achieved by using a phase-shifted sinusoidal driver signal applied to an octupole exciter. The experimental findings are reproduced by an extended Hasegawa-Wakatani model. The numerical simulation strongly supports the idea that the drive acts as a structured rotating current profile. Only if the current profile rotates at roughly the phase velocity of the preselected drift mode, control is achieved.

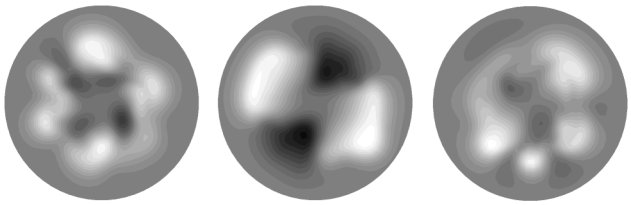

FIG. 4. Snapshots of the 2D mode structure as taken from the simulations. Gray scale plots of the density fluctuations, from left to right: Unperturbed case, corotating, and counterrotating current profile.

C. S. and T. K. gratefully acknowledge the hospitality of the Nancy plasma group during their stay. This work is supported by Deutsche Forschungsgemeinschaft under the auspices of SFB 198 "kinetics of partially ionized plasmas" and Contract No. Pi-185/14-1.

[1] W. Horton, Rev. Mod. Phys. **71**, 735 (1999).
[2] F. Wagner and U. Stroth, Plasma Phys. Controlled Fusion **35**, 1321 (1993).
[3] *Feedback and Dynamic Control of Plasmas,* edited by T. K. Chu and H. W. Hendel (American Institute of Physics, New York, 1970); K. I. Thomassen, Nucl. Fusion **11**, 175 (1971).
[4] J. S. Chiu and A. K. Sen, Phys. Rev. Lett. **83**, 5503 (1999).
[5] *Handbook of Chaos Control,* edited by H. G. Schuster (VCH-Wiley, Weinheim, 1999).
[6] T. Klinger, in [5], pp. 513–562.
[7] E. Gravier, X. Caron, and G. Bonhomme, Phys. Plasmas **6**, 1670 (1999).
[8] T. Klinger *et al.,* Phys. Rev. Lett. **79**, 3913 (1997).
[9] T. Shinbrot, Adv. Phys. **44**, 73 (1995).
[10] T. Pierre, G. Leclert, and F. Braun, Rev. Sci. Instrum. **58**, 6 (1987).
[11] T. Klinger, A. Latten, A. Piel, and G. Bonhomme, Plasma Phys. Controlled Fusion **39**, B145 (1997).
[12] T. K. Chu *et al.,* Phys. Fluids **12**, 203 (1969); E. Marden Marshall, R. F. Ellis, and J. E. Walsh, Plasma Phys. Controlled Fusion **28**, 1461 (1986).
[13] A. Latten, T. Klinger, A. Piel, and T. Pierre, Rev. Sci. Instrum. **66**, 3254 (1995).
[14] F. F. Chen, Phys. Rev. Lett. **15**, 381 (1965); H. L. Pécseli, Phys. Plasmas **25**, 1173 (1983).
[15] A. Hasegawa and M. Wakatani, Phys. Rev. Lett. **50**, 682 (1983).
[16] V. Naulin, K. H. Spatschek, S. Musher, and L. I. Piterbarg, Phys. Plasmas **2**, 2640 (1995).
[17] A. Arakawa, J. Comput. Phys. **1**, 119 (1966).
[18] G. E. Kariadakis, M. Israeli, and S. A. Orzag, J. Comput. Phys. **97**, 414 (1991).